

Steady State Thermo-Mechanics and Material Property Definition Framework for Analyzing DCLL Blanket in the Fusion Nuclear Science Facility

Sunday C. Aduloju^{*,a}, Charles Kessel^a, Dennis Youchison^a, Fayaz Rasheed^a, Paul Nogradi^a

^a *Fusion Energy Division, Oak Ridge National Laboratory, Oak Ridge, TN 37831, USA*

Fusion Engineering and Design

Abstract

A thermo-mechanics model that relies on creating the material property definition framework (MPDF) and multiphysics coupling of the heat transfer and the solid mechanics modules is developed to determine the structural integrity of the recently designed dual cooled lead lithium (DCLL) inboard blanket (IB) for the Fusion Nuclear Science Facility under steady state loads. The MPDF is called to supply fusion relevant neutron irradiation and temperature induced changes in material properties during multiphysics finite element runs, and PbLi temperature profiles are used to approximate Magnetohydrodynamics effect and the nuclear volumetric heating on the PbLi. Neutron irradiation and temperature induced reduction of the yield and ultimate strengths of F82H steel at the first wall (FW) are quantified for one year. A blanket in an assembly with gaps between blanket sectors and another blanket in an assembly with no gaps between blanket sectors, both exposed to radiation damage that lasted for one year are analyzed. Analysis using the elastic ITER structural design criteria for in-vessel components (ITER SDC-IC) design rules and a linear isotropic-hardening-type elastoplastic material model are used where most appropriate. The IB blanket with gaps between blanket sectors will withstand the steady state combined thermal and coolant loads for one year operational period but will fail if no gaps are allowed between blanket sectors. It is recommended that a gap of about 7.62 mm should be provided between IB blanket sectors during assembly which would close up during service, stop neutron streaming, reduce stresses and reduce bending of the FW into the scrape-off layer.

Key Words: Blanket, Thermo-mechanics, Multiphysics, material property definition framework, solid mechanics, heat transfer, ITER SDC-IC

* Corresponding author: Ph: (865) 307-9018; e-mail: adulojusc@ornl.gov

1. Introduction

The Fusion Nuclear Science Facility (FNSF) is being explored to provide an integrated platform for generation of relevant power plant fusion database on all components and thereby bridging the research gap between the International Thermonuclear Experimental Reactor (ITER) and DEMO [1]. The FNSF is a deuterium-tritium tokamak-based facility with a 518 MW fusion power and power gain $Q = 4$ that is designed for a plant operational lifetime of 23.5 years (~ 8.5 FPY) [2]. The plasma major radius is 4.8 m and minor radius is 1.2 m. The fusion core outer major and minor radius are about 13 m and 6.5 m respectively. A horizontal maintenance approach for the fusion core as in **Figure 1(a)** is chosen such that the tokamak is composed of 16 sectors where single full sectors could then be removed through the vacuum vessel ports [1, 3]. **Figure 1(b)** shows the cross-section of the FNSF and identifies the various components in and near the fusion core.

The first wall (FW) and blanket structure (blue) surrounds the plasma (red), absorbs the neutron energy and also a surface heat flux from the plasma. The blanket is designed to breed tritium to ensure there is sufficient tritium for nuclear fusion [4] and provide shielding for outer components from neutron damage [5]. The DCLL has been described as the most attractive blanket concept whose technology is within reach in the near term [1, 7, 10]. The DCLL IB breeding blanket with integrated helium manifold is supported at the base by the structural ring structure and vertical sliding joint that seats between the manifold and the structural ring.

The inboard blanket sector shown in **Figure 2(a)** has 321 FW helium cooled channels and it is about 7 m tall. It has 5 PbLi breeder channels in the front row and another 5 PbLi breeder channels at the back rows. The front row is demarcated from the back row by a separation plate of the blanket structure. The stiffening plates separate the 5 breeder channels in each row. Both the

stiffening plates and separation plates also provide reinforcement for the blanket structural frame. The SiC flow channel inserts (FCI) which has low thermal ($k_{\text{FCI}}=2$ W/mK) and electrical conductivities ($\sigma_{\text{FCI}}=5$ S/m) properties is fit inside the PbLi flow channels to thermally and electrically insulates the PbLi from the steel.

The helium gas cools the FW and the blanket steel structures. The PbLi liquid metal performs the function of tritium breeder and coolant, flowing within the SiC inserts, and in the small gap between the SiC and steel conduit wall. The blanket structure must accommodate the helium operating pressure of 8 MPa and PbLi inlet pressure of ~ 2 MPa. The cooling helium fluid is fed at 350°C through the helium inlet manifold to the blanket FW channels and through the grid plates (radial grid plates, separation plates and back plates), cooling the FW and steel structures. It then combines at the top, flows vertically down through the helium return manifold and exits the blanket at 475°C. The liquid PbLi flows up in the poloidal direction through the front rows of SiC flow channel inserts (FCI) and returns flowing downward through the back rows (see **Figure 2(b)**).

Reduced activated ferritic martensitic (RAFM) steel is the primary structural material candidate for fusion blanket structure due to its high temperature strength and low activation property[11, 12], and F82H type RAFM steel is considered as a prominent structural material for FNSF blanket [13-15]. However, the steel suffers from a Ductile-to-Brittle Transition Temperature (DBTT) at 350°C and creep above 550°C which dictates the operating temperature window of the blanket. Progress is being made towards developing a database for temperature, irradiation dependent, and transmutation helium induced changes in material properties for the F82H steel [16-18] and has led to recent material correlations for fusion relevant conditions[19-21]. Also, a constitutive equation was formulated in [15, 21] which relates void swelling to neutron damage, operational temperature and helium generation rate.

The objective of this work is to study the structural performance and integrity of a recently designed FNSF IB blanket under steady state fusion relevant conditions and suggest the best

assembly of the blanket sectors. A multiphysics model is built for this purpose that couples heat transfer and solid mechanics equations and allows boundary conditions that approximate CFD and MHD effects. A robust material definition framework that accommodates and simulates fusion relevant induced changes in material properties is developed and integrated into the multiphysics model. Linear elastic and elastoplastic stress strain relations are used in appropriate assembly scenarios and situations where the FW/blanket suffers insignificant/significant irradiation softening/hardening.

In the next section, we report the problem setup, Multiphysics models coupling, boundary conditions and the material property definition framework (MPDF) that simulates fusion relevant induced material changes are discussed. The correlations of temperature and irradiation to the material properties of F82H steel that are implemented as MPDF are described in Section 3. Section 4 reveals the temperature distributions produced from the heat transfer analysis and highlights the temperature and irradiation induced softening of the FW. The results of analysis of the blanket section that allows free side wall expansion and the determination of factor of safety (FOS) after one year of service using ITER-SDC-IC design rules are discussed in Section 5. Section 6 is devoted to elastoplastic analysis of the IB blanket assembled with no gaps between blanket sectors and irradiation exposure that lasted for one year. We assess the effect of irradiation induced hardening/softening on stress and strain state of the blanket.

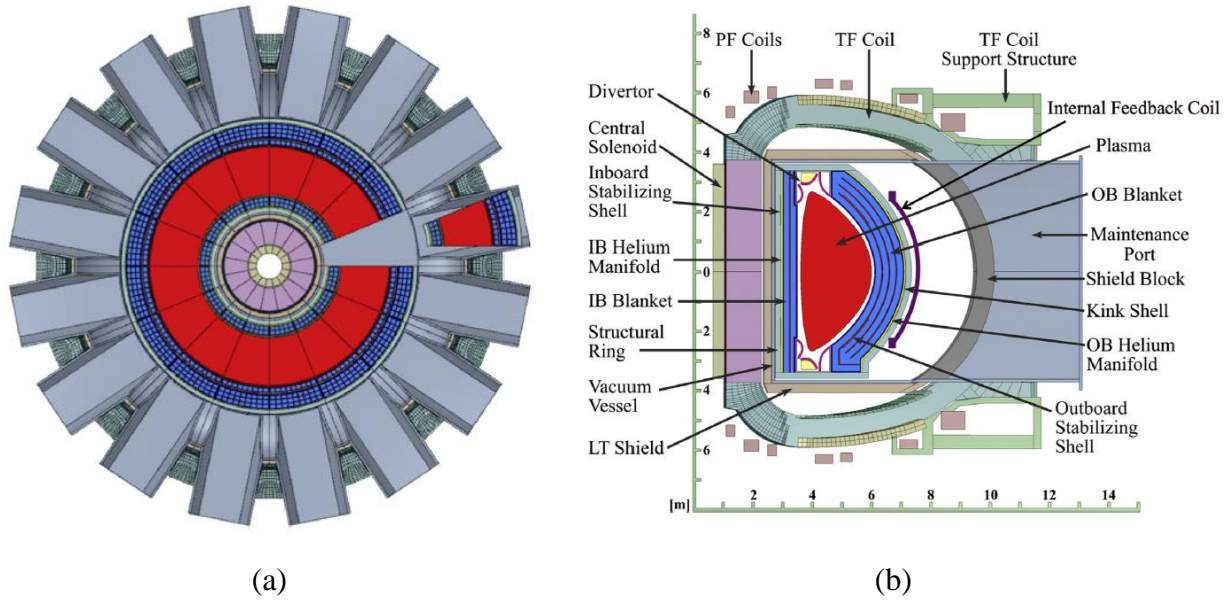


Figure 1. The FNSF power core showing in-vessel components (a)The top view showing how a sector is removed through the port (b) The cross-sectional view of the FNSF

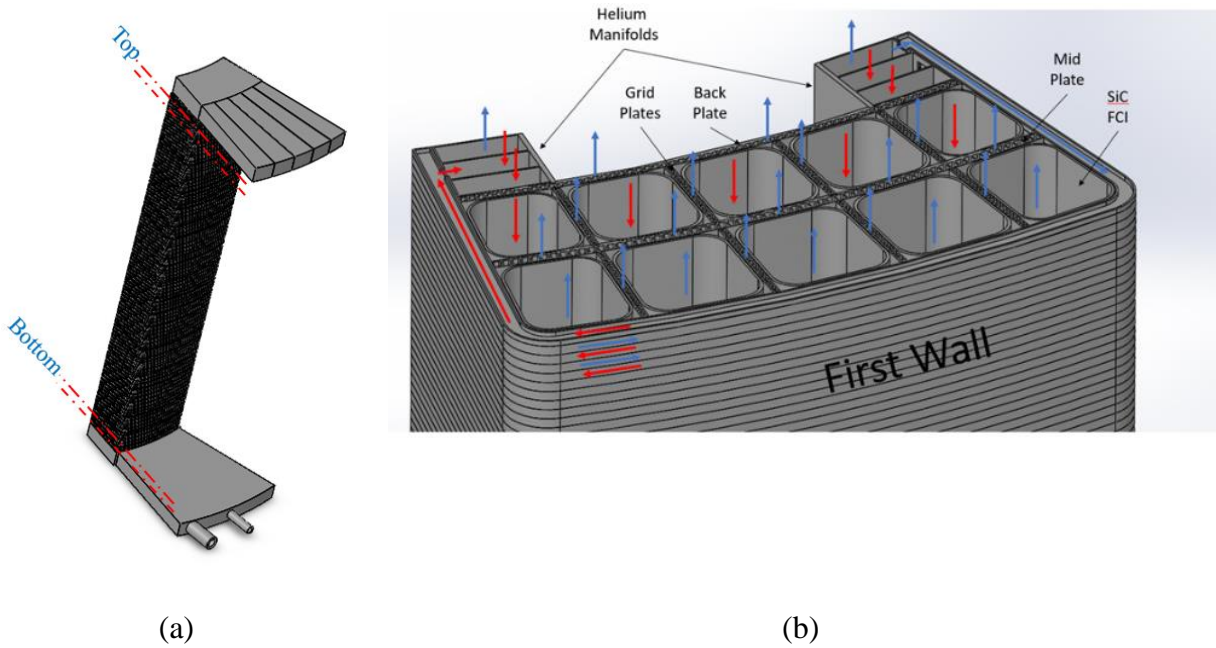
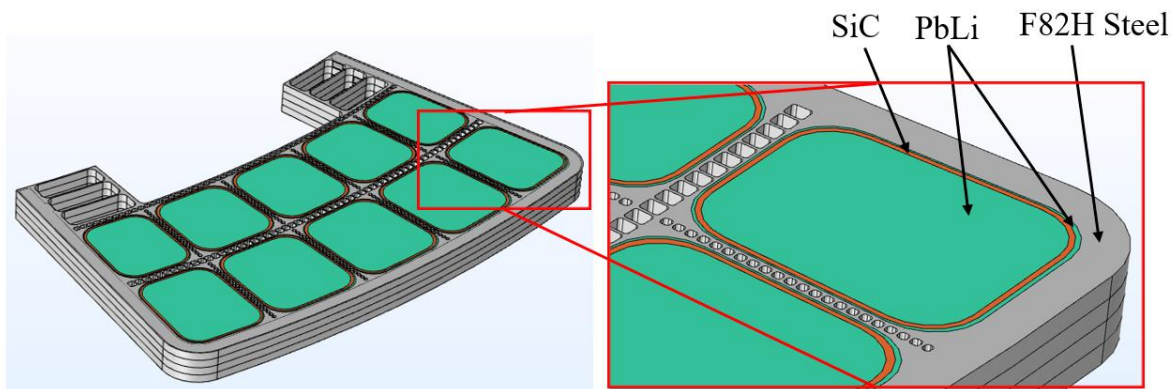


Figure 2. Inboard blanket (a) 3-dimensional view (b) internal details and flow schemes

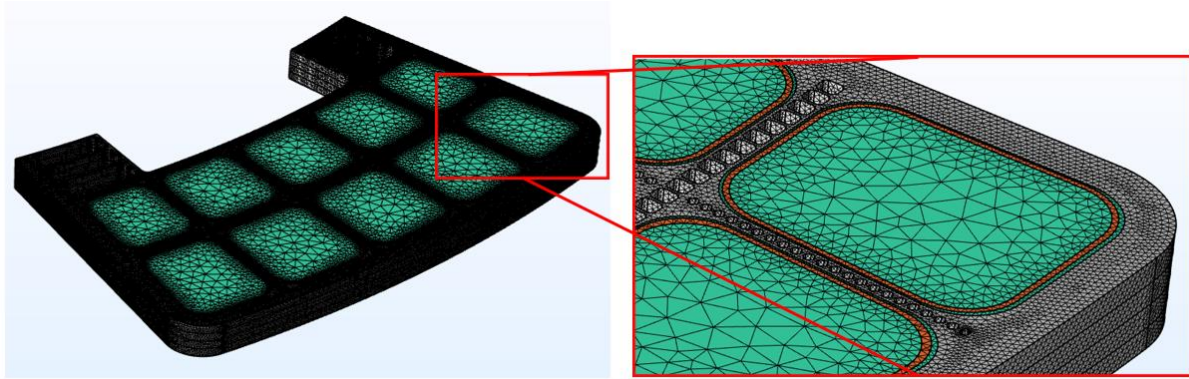
2. Problem Setup

Finite element analysis of the detailed full IB blanket sector with comparatively small features requires a great amount of computational resources. Therefore, a blanket sector piece that has four FW helium cooling channels and contains all the necessary geometrical features, materials and cooling fluids shown in **Figure 3(a)** is cut out at top and bottom of the full IB blanket sector in **Figure 2(a)**. These top and bottom blankets are analyzed to determine the structural integrity of the full IB blanket sector. Mesh refinement and convergence studies are performed to determine the number of elements required for the analysis. Finite element discretization of the model as shown in **Figure 3(b)** produced 1,217,896 unstructured tetrahedral domain elements and 457,645 triangular boundary elements. Quadratic serendipity shape functions are used to calculate the displacements while linear shape functions are used to calculate the temperatures.

A thermomechanical model that relies on the multiphysics coupling of the heat transfer equations and the solid mechanics equations is developed for analyzing the blanket model remove this line. The multiphysics coupling is developed within COMSOL Multiphysics 5.5 environment where the temperature from the heat transfer module is utilized as the thermal loads for the solid mechanics module.



(a)



(b)

Figure 3. IB blanket sector piece with four FW helium cooling channels showing (a) material assignment (b) finite element mesh

2.1 Boundary conditions

2.1.1 Heat transfer

The peak surface heat flux of 0.25 MW/m^2 is applied at the inboard blanket FW and the peak volumetric heating obtained from neutronics analysis [3, 22] that is found to decrease along the radial direction x (measured in m) from the front wall ($x = 0$) to the back wall described using eqns (1) - (2) are mapped on the blanket model. The $Q_{\text{vol-F82H}}$ (measured in W/m^3) is the volumetric heating deposited in the F82H steel blanket structure while $Q_{\text{vol-SiC}}$ (measured in W/m^3) is the volumetric heating deposited in the SiC inserts. Instead of mapping the peak volumetric heating deposited in the PbLi, the correlations provided for PbLi temperature in **Figure 4** are mapped on the PbLi model. The temperature profile of the PbLi are obtained from a separately solved coupled MHD and heat transfer blanket modeling The PbLi temperature profile approximates MHD effect and the volumetric heating on the PbLi. This self-consistent solution with temperature profile in the top, middle and bottom sections was determined by iterating between ANSYS and an MHD heat transfer code [23, 24] and found to be consistent with those

produced in [25]. Convective heat transfer coefficients of the Helium flowing through the channels are calculated by using Dittus-Boelter correlations [15, 26].

$$Q_{\text{vol-F82H}} = 9.2 \times 10^6 e^{-8.333x} \quad (1)$$

$$Q_{\text{vol-SiC}} = 8.5 \times 10^6 e^{-8.13x} \quad (2)$$

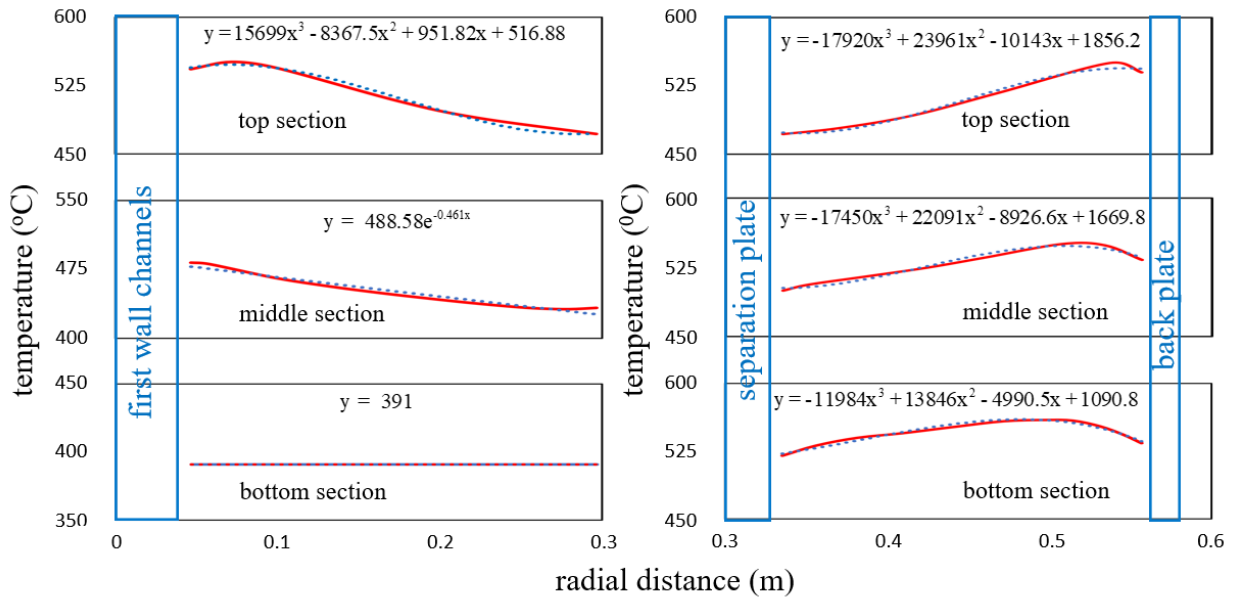


Figure 4. PbLi temperature profile in IB blanket sections

2.1.2 Solid mechanics

Free body motion is prevented by setting the displacement in a direction normal to the back of the manifold to zero (roller) and applying symmetry boundary conditions that allows displacement in a direction normal to the top surface but no displacement normal to the bottom surface. Helium gas pressure of 8 MPa is applied to FW channels, back wall (BW) and grids in the stiffening and separation plates, and PbLi pressure of 1.6 MPa is applied in the FCI channels and the steel structure interfacing walls. Two different blanket sector assembly scenarios are considered: A blanket sector assembly with side walls lower restraint limit that allows free side walls expansion and the upper restraint limit demonstrated with constrained walls. These are discussed in Section

5 and Section 6.

2.2 Material property definition framework

Spatial dependent material properties implementation, and temperature and irradiation dependent material property definition in structural analysis is uncommon because it is very complex to develop, requires nonlinear solver, can produce unstable solutions, and can require large amount of material data. A unique contribution of this work is the implementation of constitutive equations that correlate changes in neutron damage and operational temperature to material properties changes as material property definition framework (MPDF). Additionally, radiation damage is described as a phenomenon that changes across a 1-dimensional radial space. This framework is used to simulate fusion relevant induced changes in material properties within the multiphysics model.

During the multiphysics finite element runs, the MPDF is called to supply irradiation and temperature dependent material properties, a capability that is accomplished by exploiting the robust definition node in COMSOL Multiphysics where material features could be defined as expressions. Most code segments of the MPDF are implemented using analytic functions with temperature and radiation fluence as the arguments since feeding material correlations in [19] and [21] into MPDF would be straightforward. These correlations are also provided here-in for completeness. Interpolation functions could be used as substitutes for analytic functions in MPDF where raw experimental data such as those provided in [17] are preferred.

The yield strength and ultimate strength of the material selected for blanket structural frame are expressed in terms of temperature and radiation damage. Logical operators are used for creating expressions for change in material properties such as those required in the definition of the radiation softening and hardening. Spatial gradients in radiation fluence and bubble swelling are introduced by using spatial radial variable as arguments for radiation damage expression-like-variable.

3. Material Properties of F82H

The primary structural material selection for the FNSF IB blanket is F82H steel. F82H is a type of Reduced Activated Ferritic Martensitic (RAFM) steels whose main compositions are derived from the 9Cr1Mo steel and manufactured by replacing high activation elements such as Mo and Nb with low activation elements such as W, V and Ta. The ITER materials design limit data document (Appendix A, ITER SDC-IC) [27] contains brief information, physical properties, structural and thermal material properties data that could be required for studying thermo-mechanics of fusion plant in-vessel components but the document is written mostly for austenitic stainless steels and deals with low temperatures and low neutron doses. The document does not include material data for F82H steel [19] but the accurate thermo-mechanics of the IB blanket requires temperature and irradiation dependent thermal and structural properties of F82H steel. The correlations of temperature and irradiation to the material properties are provided here-in, and temperature dependent material properties are provided for use when enough neutron damage data are not available to cover the operating/design ranges.

3.1 Thermal properties of F82H steel

The correlations of the temperature T (unit in $^{\circ}\text{C}$) to the specific heat capacity C_p (unit in $\text{J}/\text{Kg}\cdot\text{K}$), thermal conductivity k (unit in $\text{W}/\text{m}\cdot\text{K}$), and thermal expansion coefficient α (unit in $1/\text{K}$) are developed for F82H steel and presented in eqns (3) - (5). These correlations are developed from material testing data in [16, 17]. Similar correlations have been provided in [19] using the same material testing data. The recent and advanced correlation tools are exploited to develop a better fit to the raw material data. The thermal conductivity is presented in **Figure 5** and it does not change much with temperature, but the thermal expansion coefficient increases with temperature.

$$C_p = 1.1932 \times 10^{-8} (T + 273)^4 - 2.7446 \times 10^{-5} (T + 273)^3 + 0.022969 (T + 273)^2 - 7.8498 (T + 273) + 1390.2 \quad (3)$$

$$k = -8 \times 10^{-9} (T + 273)^3 - 1 \times 10^{-6} (T + 273)^2 + 0.0118 (T + 273) + 28.384 \quad (4)$$

$$\alpha = -1 \times 10^{-12} (T + 273)^2 + 5 \times 10^{-9} (T + 273) + 9 \times 10^{-6} \quad (5)$$

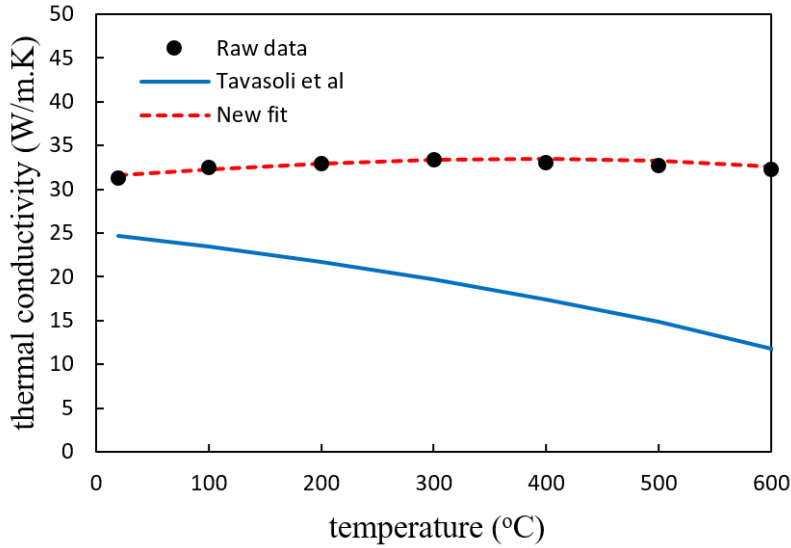


Figure 5. The temperature dependent thermal conductivity of F82H steel

3.2 Structural properties of F82H steel

The temperature dependent correlations are developed for the modulus of elasticity E (unit in GPa), Poisson ratio ν , yield strength S_y (unit in MPa), ultimate tensile strength S_u (unit in MPa), and uniform elongation ϵ_u (unit in %) of unirradiated F82H steel and presented in eqns (6) - (10) based on the data provided in the report of IEA round-robin tests [15, 17]. These correlations are consistent with the ones provided in [19] and are useful for determining the structural integrity of fusion components at the beginning of life (BOL).

$$E = -2 \times 10^{-7} T^3 + 0.0001 T^2 - 0.0778 T + 218.76 \quad (6)$$

$$\nu = 2 \times 10^{-10} T^3 - 1 \times 10^{-7} T^2 + 1 \times 10^{-5} T + 0.2897 \quad (7)$$

$$S_y(T) = 558.76 - 0.81574T + 2.7621 \times 10^{-3}T^2 - 3.476 \times 10^{-6}T^3 \quad (8)$$

$$S_u(T) = 666.44 - 0.84514T + 2.1019 \times 10^{-3}T^2 - 2.617 \times 10^{-6}T^3 \quad (9)$$

$$\varepsilon_N = 2 \times 10^{-5}T^2 - 2.08 \times 10^{-2}T + 7.2062 \quad (10)$$

The determination of the structural integrity of the blanket during service requires both temperature and irradiation dependent properties. We exploit the recent correlations provided for temperature and irradiation dependent mechanical properties of Ferritic martensitic steels [21]. Since the yield strengths at radiation fluences less than 40 dpa, are not affected by Helium concentration up to fusion relevant 10 appm He/dpa ratio, these correlations are simplified to work well for radiation fluences that are less than 40 dpa and are presented in eqn (11) - (14). At temperature $T \leq T_s$, neutron irradiation hardening of the steel occurs which causes the yield strength of the steel to increase. The strengthening or irradiation hardening ΔS_{yIH} of F82H steel is expressed in terms of the temperature T (unit in °C) and neutron damage ϕ (unit in dpa) in eqn (11).

$$\Delta S_{yIH}(T, \phi) = (1951.4 - 4.9666T) \left[1 - \exp\left(\frac{-\phi}{\phi_0}\right) \right]^{1/2} \quad (11)$$

Above hardening-softening transition temperature $T_s = 400^\circ C$, there is irradiation softening ΔS_{yIS} of the F82H steel which it is given by eqn (12).

$$\Delta S_{yIS}(T, \phi) = (26.18 - 0.08T) \sqrt{\phi} \quad (12)$$

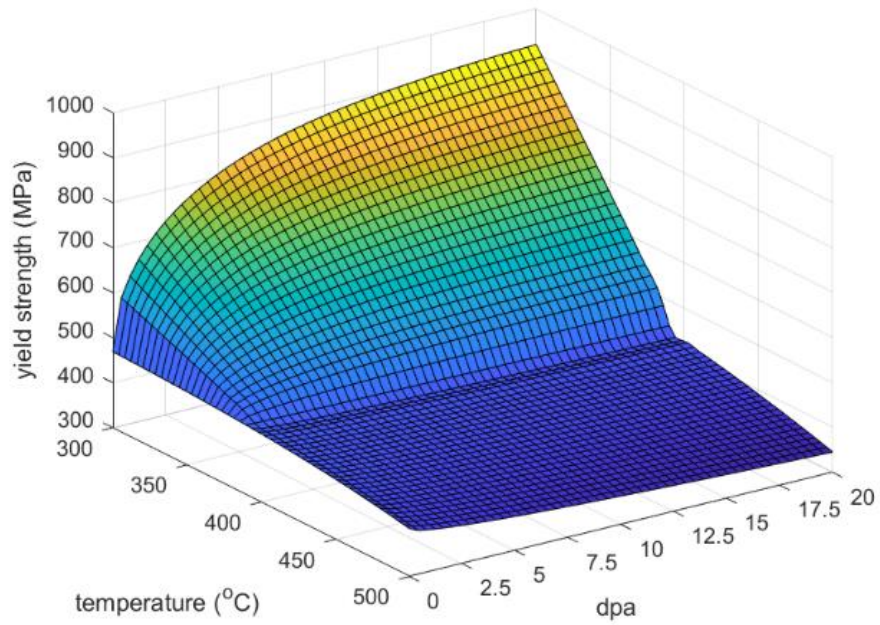
The hardening or softening ΔS_{yI} of the steel due to irradiation is used to calculate the yield strength $S_{y,irr}$ and ultimate strength $S_{u,irr}$ of the irradiated F82H steel in eqns (13) and (14). The attention of the reader is drawn to the ratio of change in ultimate strength to change in yield strength [15] that is expressed in terms of the of Helium concentration (HC, unit in appm) in eqn (14).

$$S_{y,irr}(T, \phi) = S_y(T) + \Delta S_{yl}(T, \phi) \quad (13)$$

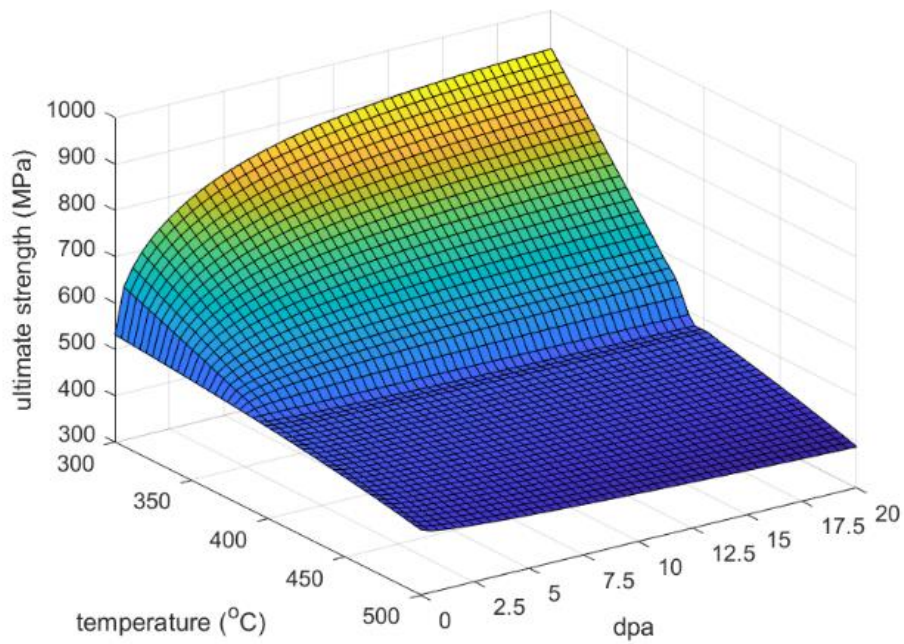
$$S_{u,irr}(T, \phi, HC) = S_u(T) + (5 \times 10^{-5} HC + 0.8248) \Delta S_{yl}(T, \phi) \quad (14)$$

The radiation exposure required for 80% of initial saturation hardening $\phi_o = 6.5$ dpa are required to determine the change in the strengths due to neutron irradiation. The analyses in later sections employ fusion relevant 10 appm He/dpa ratio.

The 3-dimensional plots of the temperature and irradiation dependent yield strength and ultimate strength produced using eqns (8), (9) and (11) - (14) are presented in **Figure 6(a)** and **Figure 6(b)**. The yield strength decreases monotonically with increase in temperature when the steel is unirradiated. The irradiated structural material behavior follows hardening that decreases with increase in temperature, transitions to softening at 400°C which later increases with temperature. At lower temperature (below 360°C) and lower neutron irradiation, there is sharp increase in the yield strength with increase in neutron irradiation and later transitions to slight increase as the neutron dose approaches 20 dpa. The transition to slight increase in yield strength due to saturation in the irradiation induced microstructural defects is expected to continue up to 40 dpa.



(a)



(b)

Figure 6. F82H temperature and irradiation dependent structural properties (a) yield strength (b) ultimate strength

Beyond 40 dpa, Helium concentration would cause additional hardening due to microstructural changes such as precipitate hardening. At high irradiation, the strain hardening capacity (the ratio of the ultimate strength to yield strength) at lower temperature approaches 1 and is smaller than strain hardening capacity at higher temperature.

3.3 Radiation damage dose & bubble swelling

The results of the neutronics analysis [2, 15] that was performed on the FNSF design and presented in **Figure 7(a)**, shows that the irradiation damage dose (dpa/yr) on the inboard blanket is found to decrease along the radial direction from the front wall to the back wall. The irradiation damage during service is calculated from this damage dosage and mapped on the IB blanket structure to allow us to include the effects of spatial gradients in radiation damage on the structural integrity of the blanket structure.

A simplified irradiation dependent linear model for bubble swelling f_v (unit in %) in eqn (15), that works well for radiation fluence less than 50 dpa, is used to capture the variation of neutron-induced bubble swelling with respect to irradiation damage at all temperatures in this work. The neutron-induced void and bubble swelling effects are modeled as an inelastic isotropic strain ε_{kk}^s according to eqn (16). The definition of the bubble swelling introduces a spatial gradient in material degradation and affects the stress state and deformation of blanket.

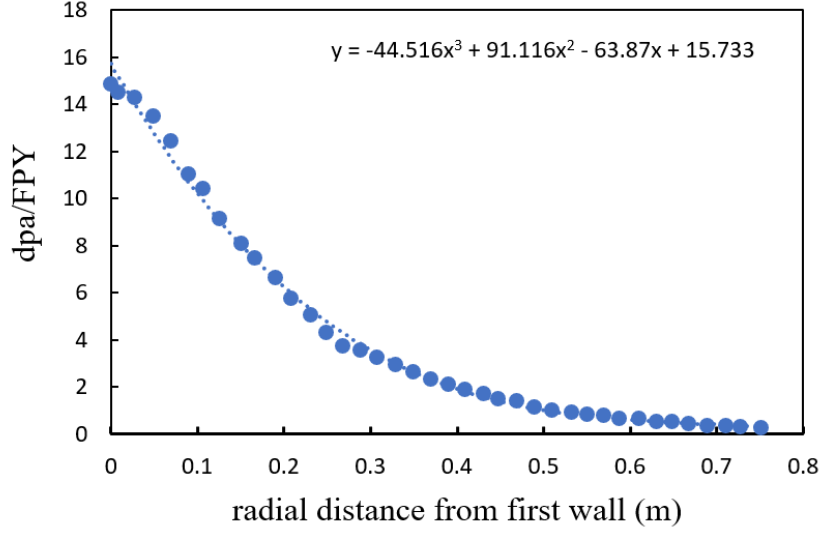


Figure 7. Radiation damage rate on IB blanket [15]

$$f_v = 0.0078\phi \quad (15)$$

$$\varepsilon_{11}^s = \varepsilon_{22}^s = \varepsilon_{33}^s = f_v/3 \quad (16)$$

4 Blanket Temperatures and Irradiation Softening at First Wall

The temperature accompanied by irradiation is an important part for determining the damage criteria or structural integrity of the blanket structure. The temperature distributions that are produced from the heat transfer analysis are combined with the one full power year irradiation damage data from the neutronics analysis and supplied to the MPDF to determine if some regions of the F82H steel blanket structural frame have undergone irradiation softening or hardening. We present the combined irradiation damage and temperature induced reduction in the yield and ultimate strengths of F82H steel at the FW after one year.

4.1 Blanket and first wall temperatures

At the bottom blanket in **Figure 8(a)**, the temperature of PbLi entering the front SiC insert is lower than the temperature of the PbLi leaving the back insert. At the top blanket in **Figure 8(b)**, the temperature of the PbLi in the front insert decreases further away from the front wall while the

temperature of the PbLi in back insert of the top blanket is uniformly distributed due to strong fluid mixing at the top of the IB blanket sector. The highest PbLi temperatures are 544°C near the FW of the top blanket, and 549°C at the back insert of the bottom blanket.

The temperature on the blanket structure increases from 350°C from the bottom of the IB blanket in **Figure 9(a)** to 526°C at the top of the IB blanket in **Figure 9(b)**. Higher heat is transferred through the FW of the blanket bottom because the FW is cooled by the cooler incoming Helium gas. The temperature of the inner supporting structures (radial grid plates, separation plates and back plates) of the blanket increases in the vertical direction from the bottom to the top of the blanket and the hotter return helium gas is responsible for the sharp temperature rise in the return manifold of the bottom blanket.

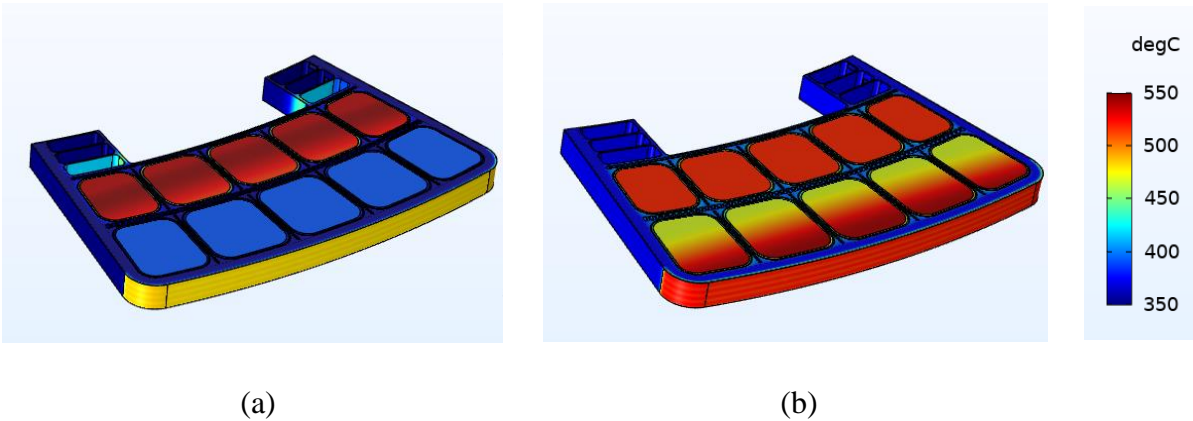
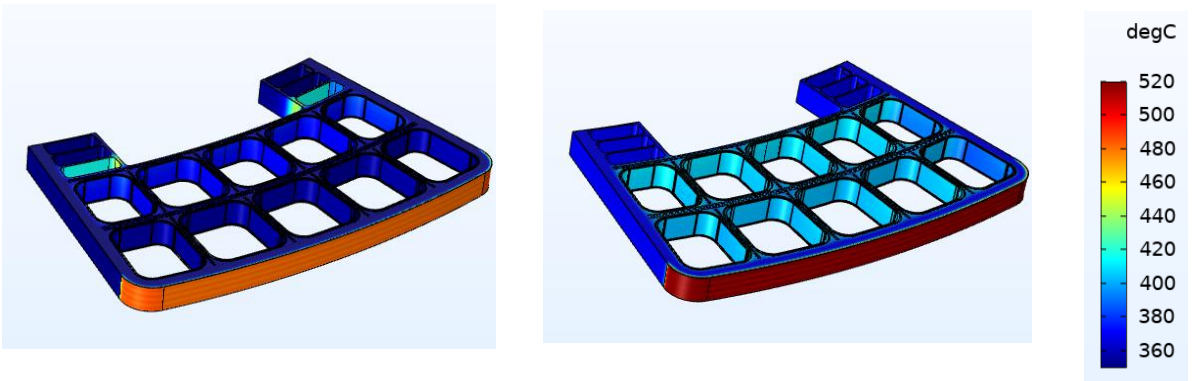


Figure 8. Temperature contour plots on the blanket sector piece at (a) bottom (b) top



(a)

(b)

Figure 9. Temperature contour plots on the frame of blanket sector piece at (a) bottom (b) top

4.2 Irradiation softening at first wall

The yield and ultimate strengths of the F82H steel at the FW at BOL and after one year is presented in **Table 1**. The irradiation softening is responsible for reduction of yield strengths at the FW after one year. Neutron damage of 15 dpa at 487°C caused the yield strength of the FW at the bottom blanket to reduce from 415 MPa (at BOL) to 366 MPa. The ultimate strength of the F82H steel at the FW of the bottom blanket is reduced from 451 MPa by 41 MPa. There is also yield strength reduction of the F82H steel at the FW of the top blanket from 388 MPa (at BOL) to 327 MPa due to neutron damage of 15 dpa at 526°C. The ultimate strength of the F82H steel at the FW of the top blanket is reduced from 423 MPa by 51 MPa. Therefore, the combined irradiation damage and temperature will reduce the yield and ultimate strengths of F82H steel at the FW on average by about 55 MPa and 46 MPa after one year.

Table 1. Yield and ultimate strengths of the FW at BOL and after one year

FW of blanket	BOL		One year	
	S _y (MPa)	S _u (MPa)	S _y (MPa)	S _u (MPa)
Bottom	415	451	366	410
Top	388	423	327	372

5. Elastic ITER-SDC-IC Analysis of IB Blanket with Free Side Walls

Component classifications using existing codes for the construction of nuclear power plants do not necessarily apply to the fusion in-vessel components since these codes do not address the effects of irradiation on the in-vessel components. ITER SDC-IC was developed from RCC-MR code, ASME and European harmonized standards and it contains rules for design of in-vessel components used in a nuclear fusion plant. The ITER SDC-IC design rules are used to analyze

monotonic damage in the blanket [28].

The multiphysics model developed earlier is used to analyze the IB blanket that is assembled with gaps between blanket sectors and exposed to radiation damage that lasted for one year. Free side walls expansion is allowed on the top and bottom blankets to simulate blanket assembly with gaps between IB blanket sectors, and elastic stress-strain relationship is assumed. Spatial gradients of radiation fluence are accounted for by mapping the neutron irradiation damage in **Figure 7** that varies from 15 dpa at the FW to 0.25 dpa at the BW on the IB blanket structure. Heat transfer and solid mechanics boundary conditions that are discussed earlier are applied and temperature dependent material properties used. The temperature, displacements and stresses are calculated, and stress intensities evaluated are compared to the allowable to obtain FOS.

5.1 Stresses and displacements

The temperature variation across the blanket structure produces thermal stresses due to uneven thermal expansion of the blanket, and the fluid pressure loads produce additional mechanical stresses. The maximum stress on the bottom blanket is 354 MPa and the stress contour striations on the FW of the bottom blanket in **Figure 10(a)** are present due to high stress concentrations at the cooling channels corners. **Figure 10(b)** shows the stress contour plot on the top blanket with high stresses where the FW is attached to the stiffeners and the maximum stress of 372MPa is at the FW corners.

The deformation of the IB blanket in **Figure 11** is predominantly governed by thermal expansion due to volumetric and surface heating of the blanket. The displacements contour plots in **Figure 11(a)** and **Figure 11(b)** show that the highest displacements at the bottom and top of the blanket structure are 3.81 mm and 4.63 mm and are located at corners of the plasma FW. If a gap of 7.62mm which is twice the maximum displacement (3.81 mm) at the bottom of the blanket sector is allowed between neighboring blanket sector at the beginning of life, the gap will close up during service and prevent neutron streaming. But if the gap that is twice the highest displacement

at the top is provided between neighboring blanket sectors at the beginning of life, there will still be gap at the bottom of the blanket sector during service thereby allowing neutron to stream through the FW.

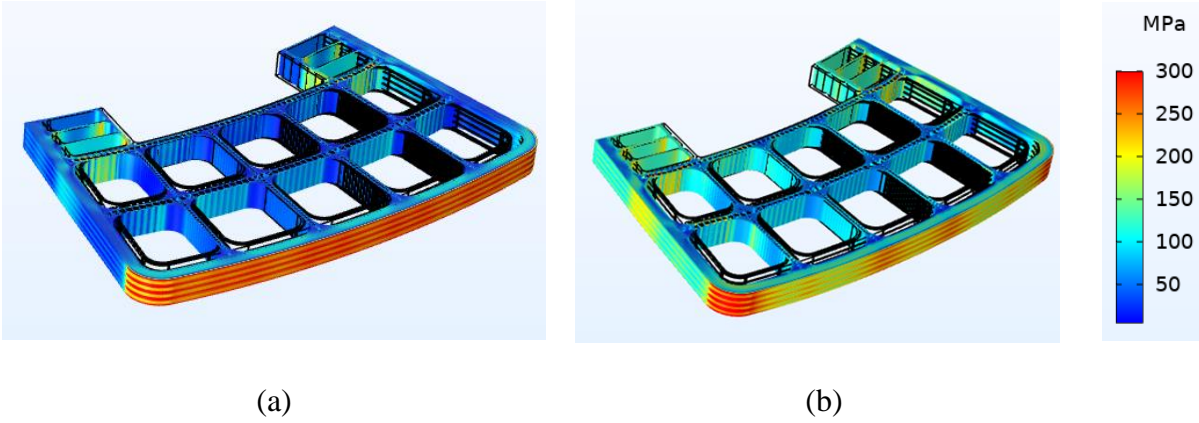


Figure 10. Stress contour plots (on deformed configuration $\times 10$) obtained from applied free side walls on blanket sector piece at the (a) bottom (b) top

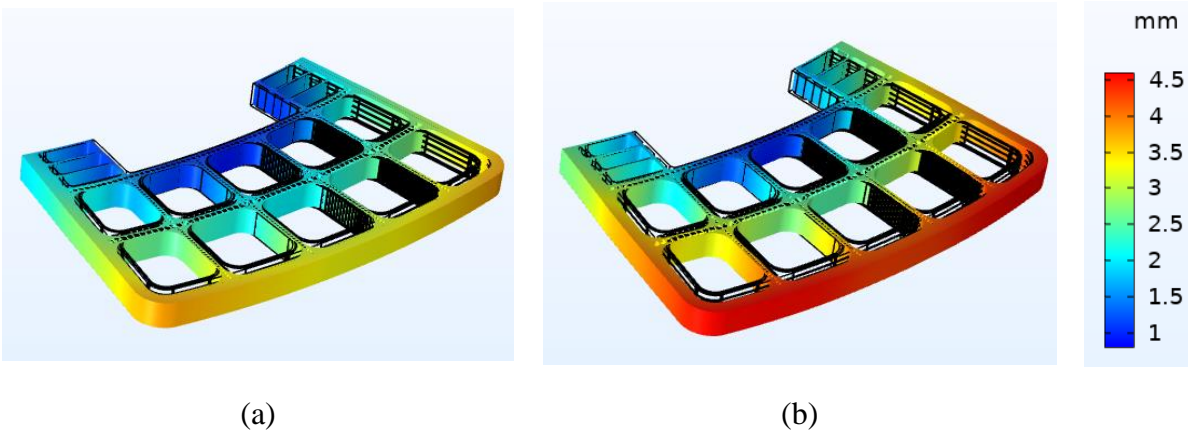


Figure 11. Displacement contour plots (on deformed configuration $\times 10$) obtained from applied free side walls on blanket sector piece at the (a) bottom (b) top

5.2 Factor of Safety based on ITER-SDC-IC

The IB blanket structural integrity for ductile damage modes such as necking and plastic instability, and non-ductile damage modes such as plastic flow localization and ductility exhaustion induced local fracture is evaluated by carrying out two different additional analyses on

the blanket model. Mechanical loads consisting of the fluid pressure are only applied to the blanket model in the first analysis to calculate the primary stress (P) while secondary stress is calculated from the second analysis of the blanket which accounts for the effect of thermal loads only. Elastic ITER-SDC-IC design rules are used to evaluate the FOS for protection against Monotonic-type damage under SDC-IC criteria level A (normal operating service conditions) according to **Table 2**.

Table 2. ITER-SDC-IC design rules for Monotonic-type damage

Damage limits	Factor of safety/design rules
Necking and plastic instability	$FOS_{NPI} = \frac{K_{eff} S_m(T, \phi t)}{P_m + P_b} \geq 1$
Immediate plastic flow localization	$FOS_{PI} = \frac{S_e(T, \phi t)}{P_m + Q_m} \geq 1$
Ductility exhaustion	$FOS_{De} = \frac{S_d(T, \phi t, r_3)}{P_m + P_b + Q} \geq 1$
$3S_m$ criteria	$FOS_{PQ} = \frac{3S_m(T, \phi t)}{P + Q} \geq 1$

In the table above, a bar denotes effective stress. P_m is the general primary membrane stress, P_b is primary bending stress, Q is the secondary stress, Q_m is the secondary membrane stress and K_{eff} is bending shape factor (1.5 for solid rectangular cross section). The general primary membrane stress instead of the local primary membrane stress is used for the calculation of the FOS because there is no gross structural discontinuity in the blanket model that could produce additional membrane stress above the general primary membrane stress. The allowable primary membrane stress S_m , the allowable primary plus secondary membrane stress intensity S_e and the

allowable total stress intensity S_d in the table are evaluated as function of temperature and neutron damage in eqns (17) - (19).

$$S_m(T, \phi) = \min \left[\begin{array}{l} \frac{2}{3} S_{y,\min}(RT, 0), \frac{2}{3} S_{y,\min}(T_m, 0), \frac{2}{3} S_{y,\text{irr}}(T_m, \phi_m), \frac{1}{3} S_{u,\min}(RT, 0), \\ \frac{1}{2.7} S_{u,\min}(T_m, 0), \frac{1}{2.7} S_{u,\text{irr}}(T_m, \phi_m) \end{array} \right] \quad (17)$$

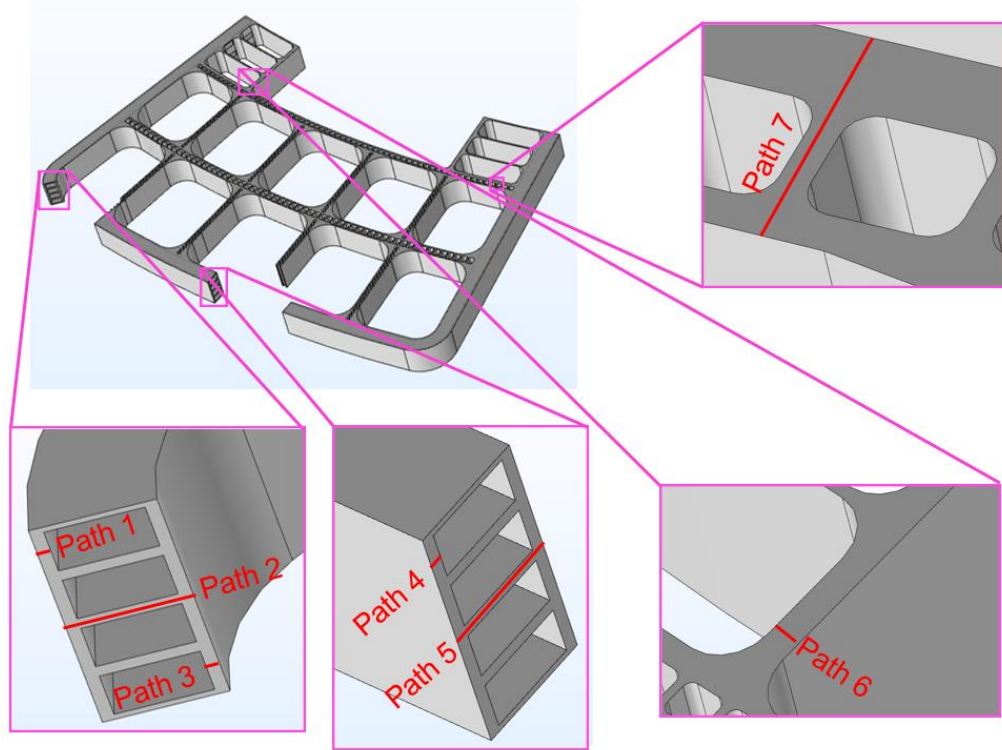
$$S_e(T, \phi) = \begin{cases} \frac{1}{3} S_{u,\text{irr}}(T_m, \phi_m) + \frac{0.5E}{r_1} (\varepsilon_u(T_m, \phi_m) - 0.02) & \text{if } \varepsilon_u(T_m, \phi_m) \geq 2\% \\ \frac{1}{3} S_{u,\text{irr}}(T_m, \phi_m) & \text{if } \varepsilon_u(T_m, \phi_m) < 2\% \end{cases} \quad (18)$$

$$S_d(T, \phi) = \frac{2}{3} \left[S_{u,\text{irr}}(T_m, \phi_m) + \frac{E\varepsilon_{ir}(T_m, \phi_m)}{r_3 \times TF} \right] \quad (19)$$

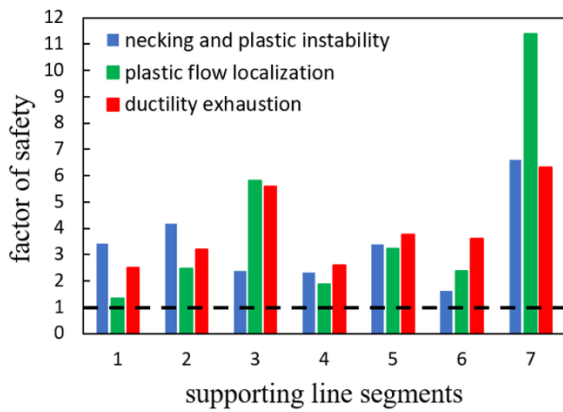
In the above equations, RT is the room temperature, T_m is thickness-averaged temperature and ϕ_m thickness-average neutron damage. Also, ε_u is the minimum uniform elongation, r_1 and r_3 are elastic follow up factors. For level A criteria, $r_1 = 4$ could be used as conservative value but could be explicitly derived according to IC2161. The elastic-follow-up factor $r_3 = \infty$ for $\varepsilon_u \leq 0.002$ or $r_3 = 4$ for $\varepsilon_u > 0.002$. TF is the triaxiality factor. ε_{ir} is the minimum true strain at rupture. The Criterion excluding peak stress commonly used to evaluate the FOS for protection against damage due to ductility exhaustion is employed [3, 29-31] and the second term for calculating the total allowable stress intensity is neglected in this analysis because there are not enough data for evaluating the minimum true strain to rupture.

The stress intensities are evaluated on the supporting line segments that are drawn on critical areas (areas with high total, membrane or bending stresses) of the top and bottom IB blanket and compared with the allowable stress intensities that are evaluated for one year of blanket operation. The results presented in **Figure 12** show that the FOS for all damage limits considered are greater

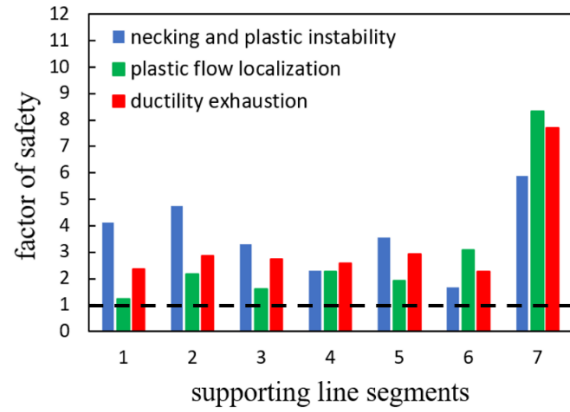
than 1 which indicates that the blanket design can withstand all steady state loads for one year operation. The blanket design generally has the lowest margin of safety for plastic flow localization, and highest margin of safety for necking and plastic instability.



(a)



(b)



(c)

Figure 12. ITER-SDC-IC criteria for damage on IB blanket showing (a) location of supporting line segments (b) FOS plots on bottom piece (c) FOS plots on top piece

6. Elastoplastic Analysis of Blanket with Constrained Side Walls

The multiphysics model is used to determine the structural integrity of the IB blanket that is assembled with no gaps between blanket sectors and exposed to radiation damage that lasted for one year. The top and bottom blankets are constrained on the blanket side walls to simulate blanket assembly with no gaps between IB blanket sectors.

Linear isotropic-hardening-type elastoplastic model (with small strains assumption) is used instead of the linear elastic stress-strain relation to prevent spurious high stresses that can be produced from large strains. The tangent modulus is described in terms of the temperature and radiation dependent material properties as in eqn (20). However, the slope of the tangent modulus does not terminate at the ultimate strength and this present study does not include implementation of damage model that could capture fracture behavior. Therefore the blanket will fail at the regions where the stresses are greater than the ultimate strength and damage models [32, 33] that could capture onset and progressive fracture of the blanket can be pursued in future publications.

$$E_t = \frac{S_{u,irr} - S_{y,irr}}{\epsilon_u - \frac{S_{y,irr}}{E}} \quad (20)$$

The current analysis makes use of the temperature-only dependent uniform elongation in the determination of the tangent modulus because temperature and radiation dependent correlations for uniform elongation requires additional experimental data that are not currently available [15, 34]. However, it is noted that the calculated uniform elongation values can reduce significantly with the inclusion of radiation effects.

6.1 Stresses and displacements

The stress contour plots on the blanket in **Figure 13** show high stresses at the plasma facing FW with stiffening ribs, the separation plate, and the back plate. The stresses on sidewalls of the bottom blanket in **Figure 13(a)** are lower than the stresses on the top blanket in **Figure 13(b)** but the stresses on FW of the bottom blanket are higher than the stresses on the top blanket. The

maximum stresses on the bottom and top blankets are 582 MPa and 596MPa respectively. The stress concentrations at the Helium cooling channel corners that appears as stress contour striations on the FW of the bottom blanket in **Figure 10(a)** are reduced significantly in **Figure 13(a)**. The reduction of the stress contour striations can occur due to change of the deformation mode of the FW from expansion-type to bending-type deformation.

Some regions of the blanket frame with temperature higher than 400°C such as the FW undergoes irradiation softening. The ultimate strengths of the F82H steel at the FW of the bottom and top blankets are reduced to 410 MPa and 372 MPa by neutron irradiation and temperature but stresses on the FW with stiffeners are greater than the ultimate strength. Also, stresses are found to be greater than the temperature and irradiation dependent ultimate strengths that are evaluated on some blanket regions even when they undergo irradiation hardening. The blanket will fail at the FW with stiffeners, at the separation plate and at the back plate.

The stress state across the blanket with constrained side walls are generally greater than the stress state across the blanket with free side walls. These higher stresses are present due to the side walls constraint that prevents free side wall expansion in the former. Therefore, blanket sector assembly with gaps between blanket IB blanket sector is desirable but this gap should close during service to be able to stop neutron streaming while reducing bending of the FW into the scrape-off layer. A gap of about 7.62 mm gap should be provided between IB blanket sectors during assembly since the maximum displacement on the sidewall of the blanket with free side walls that will close up during service is 3.81mm.

The displacements on the bottom blanket in **Figure 14(a)** are lower than the displacements on the top blanket in **Figure 14(b)** and the maximum displacements on the bottom and top blankets are 11.60 mm and 14.40 mm. The deformation of the blanket follows a bending-type deformation mode at the FW with maximum deformation at the middle.

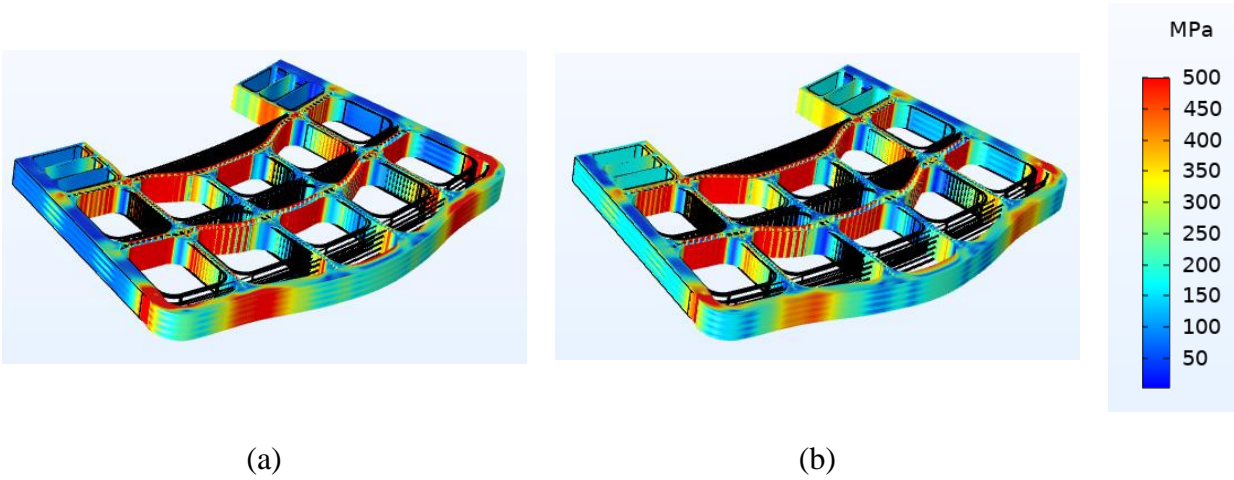


Figure 13. Von-Mises stress contour plots (on deformed configuration $\times 10$) obtained from applied constrained side walls on blanket sector piece at the (a) bottom (b) top

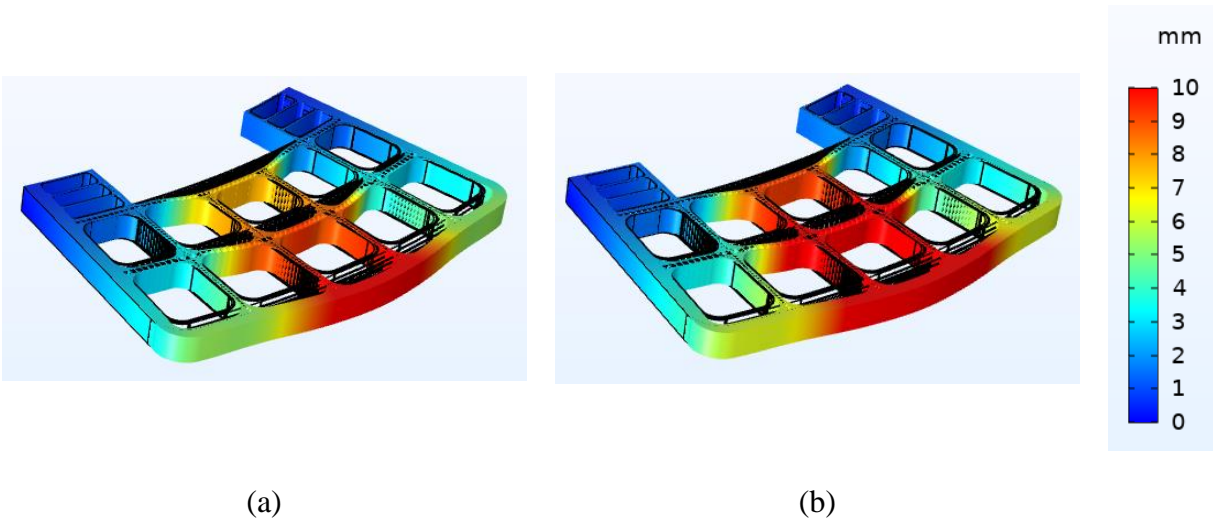


Figure 14. Displacement contour plots (on deformed configuration $\times 10$) obtained from applied constrained side walls on blanket sector piece at the (a) bottom (b) top

6.2 Plastic strains

The effective plastic strain contour plots in **Figure 15** show regions of the blanket that have undergone plastic deformation due to stresses that are greater than yield strengths. The plastic strains on the bottom blanket in **Figure 15 (a)** are generally lower than the plastic strains on the

top blanket in **Figure 15 (b)** but the maximum plastic strains on the bottom and top blankets are 2.85 % and 2.77 %. The plastic strain contour plots show that the plastic strains are significantly higher at the separation plate and the back plate than other regions of the blanket thereby providing an indication of where the blanket may fail.

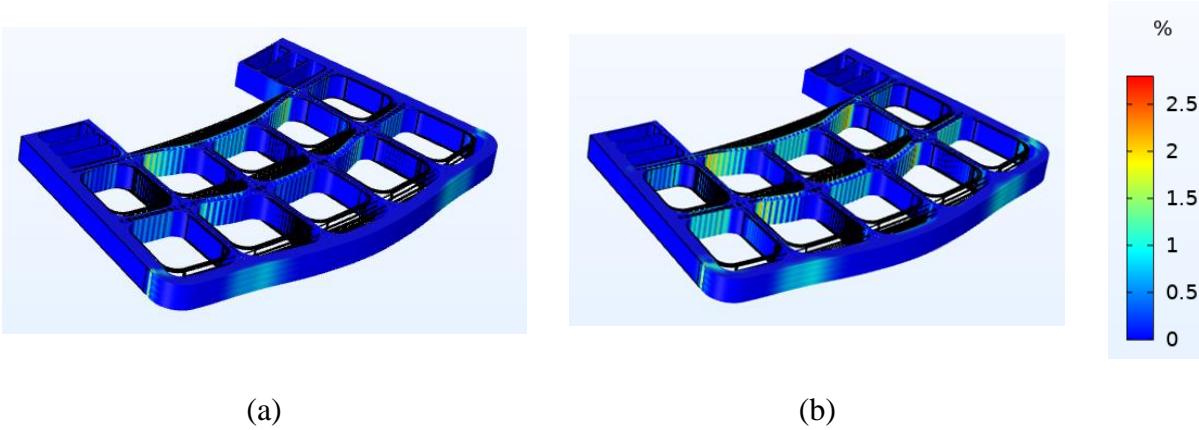


Figure 15. Plastic strain contour plots (on deformed configuration $\times 10$) obtained from applied constrained side walls on blanket sector piece at the (a) bottom (b) top

7. Conclusion

Heat transfer and solid mechanics physics are coupled and a material property definition framework (MPDF) that simulates fusion relevant induced changes in material properties is created within the multiphysics model. The model is used for steady state thermo-mechanics of the DCLL IB blanket sector that was designed for use in FNSF. A blanket piece that has 4 FW helium cooling channels is cut from the top and bottom of the full blanket sector and subjected to mechanical loads due to coolant fluids pressures, and thermal stress that are produced from thermal expansion. The spatial gradient of the radiation damage and temperature across the radial distance of the blanket makes the problem nontrivial because it causes material properties, and damage phenomenon such as swelling to change across material points in the model. The MPDF is developed and integrated into the multiphysics model to simulate the radiation and temperature induced material properties changes. Temperature dependent material properties are provided for

use in the analysis when enough neutron damage data are not available to cover the operating/design ranges.

The combined irradiation damage and temperature will reduce the yield and ultimate strengths of F82H steel at the FW on average by about 55 MPa and 46 MPa after one year. The first analysis is performed to determine the structural integrity of the blanket assuming gaps between blanket sectors (free side walls) and exposure to radiation damage that lasted for one year. The maximum stress produced is 372MPa and the blanket deforms dominantly by expansion with the highest displacements at the bottom and top of the blanket structure being 3.81 mm and 4.63 mm and are located at corners of the plasma FW. The FOS calculated using ITER-SDC-IC design rules shows that the IB Blanket with free side walls would sustain the steady state operational loads for one year.

Blanket assembly with no gaps between blanket sectors is desirable because it prevents direct neutron streaming to the outer components. The second analysis is performed to determine the structural integrity of the blanket assuming no gaps between blanket sectors (constrained side walls) and exposure to radiation damage that lasted for one year. The current analysis makes use of the temperature-only dependent uniform elongation in the determination of the tangent modulus because temperature and radiation dependent correlations for uniform elongation requires additional experimental data that are not currently available. The maximum stress on the blanket is 596 MPa and the IB blanket could fail at the FW because of the irradiation softening, large deformation, and high stresses at the FW. The deformation of the blanket follows a bending-type deformation mode at the FW that causes maximum deformation of 14.4 mm at the middle of the FW of the top piece IB blanket sector. The maximum plastic strain of the IB blanket sector with no gaps between sectors assembly is 2.85 %. The blanket would fail at the FW with stiffeners, separation plate and back plate due to large stresses that are greater than the ultimate strengths.

During assembly, a gap of about 7.62 mm should be provided between blanket sectors which

would close up during service, stop neutron streaming, reduce stresses and reduce bending of the FW into the scrape-off layer.

Declaration of Competing Interest

The authors declare that they have no known competing financial interests or personal relationships that could have appeared to influence the work reported in this paper.

Acknowledgements

This work was supported by the Oak Ridge National Laboratory managed by UT-Battelle, LLC for the U.S. Department of Energy (DOE) under contract number DEAC05-00OR22725. The U.S. government retains and the publisher, by accepting the paper for publication, acknowledges that the U.S. government retains a nonexclusive, paid-up, irrevocable, worldwide license to publish or reproduce the published form of this manuscript, or allow others to do so, for U.S. government purposes. DOE will provide public access to these results of federally sponsored research in accordance with the DOE Public Access Plan (<http://energy.gov/downloads/doe-public-access-plan>).

References

1. Kessel, C., et al., *Overview of the fusion nuclear science facility, a credible break-in step on the path to fusion energy*. Fusion Engineering and Design, 2018. **135**: p. 236-270.
2. Davis, A., et al., *Neutronics Aspects of the FESS-FNSF*. Fusion Engineering and Design, 2018. **135**: p. 271-278.
3. Huang, Y., et al., *Multiphysics modeling of the FW/Blanket of the US fusion nuclear science facility (FNSF)*. Fusion Engineering and Design, 2018. **135**: p. 279-289.
4. Abdou, M., et al., *Blanket/first wall challenges and required R&D on the pathway to DEMO*. Fusion Engineering and Design, 2015. **100**: p. 2-43.
5. Kessel, C., et al., *The Compactness and Inboard Radial Build of Fusion Nuclear Devices*. Fusion Science Technology, 2021: p. 1-13.
6. Merrill, B., et al., *Normal operation and maintenance safety lessons from the ITER US PbLi test blanket module program for a US FNSF and DEMO*. Fusion Engineering and Design, 2014. **89**(9-10): p. 1989-1994.
7. Smolentsev, S., et al., *R&D needs and approach to measure progress for liquid metal blankets and systems on the pathway from present experimental facilities to FNSF*. Fusion

- Science Technology, 2015. **68**(2): p. 245-250.
8. Smolentsev, S., et al., *MHD thermohydraulics analysis and supporting R&D for DCLL blanket in the FNSF*. Fusion Engineering and Design, 2018. **135**: p. 314-323.
 9. El-Guebaly, L., et al., *TBM/MTM for HTS-FNSF: an innovative testing strategy to qualify/validate fusion technologies for US DEMO*. Energies, 2016. **9**(8): p. 632.
 10. Wong, C., et al., *An overview of the US DCLL ITER-TBM program*. Fusion Engineering and Design, 2010. **85**(7-9): p. 1129-1132.
 11. Hirose, T., et al., *Evaluation of fatigue properties of reduced activation ferritic/martensitic steel, F82H for development of design criteria*. Fusion Engineering and Design, 2020. **160**: p. 111823.
 12. Muroga, T., M. Gasparotto, and S. Zinkle, *Overview of materials research for fusion reactors*. Fusion Engineering and Design, 2002. **61**: p. 13-25.
 13. Blanchard, J., C. Martin, and W. Liu, *Effect of ELMS and disruptions on FNSF plasma-facing components*. Fusion Engineering and Design, 2018. **135**: p. 337-345.
 14. Wallace, G., T. Bohm, and C. Kessel, *Multiphysics Simulations of a Steady-State Lower Hybrid Current Drive Antenna for the FSNF*. Fusion Science Technology, 2021. **77**(2): p. 159-171.
 15. Ghazari, A., et al., *Radiation effects on stress evolution and dimensional stability of large fusion energy structures*. Fusion Engineering and Design, 2021. **172**: p. 112756.
 16. Shiba, K.J.J., Tokyo, Japan, *Report of JAERI-Tech-97-038*. 1998.
 17. Shiba, K., et al., *Properties of low activation ferritic steel F82H IEA heat. Interim report of IEA round-robin tests. 1*. 1997.
 18. Dai, Y., G. Odette, and T. Yamamoto, *1.06-The effects of helium in irradiated structural alloys*. Comprehensive Nuclear Materials, 2012: p. 141-193.
 19. Tavassoli, A.-A., et al., *Materials design data for reduced activation martensitic steel type F82H*. Fusion Engineering and Design, 2002. **61**: p. 617-628.
 20. Yamamoto, T., et al., *On the effects of irradiation and helium on the yield stress changes and hardening and non-hardening embrittlement of ~ 8Cr tempered martensitic steels: Compilation and analysis of existing data*. Journal of nuclear materials, 2006. **356**(1-3): p. 27-49.
 21. Yamamoto, T. and G.R. Odette, *Constitutive models for hardening of tempered martensitic steels at 300 to 500 ° up to high dpa and helium*. . Technical Report DOE/ER-0313/68 Fusion Reactor Materials Semiannual Report, Oak Ridge, TN, 2020. **68**.
 22. Bohm, T.D., et al., *Initial Neutronics Investigation of a Liquid-Metal Plasma-Facing Fusion Nuclear Science Facility*. Fusion Science Technology, 2019. **75**(6): p. 429-437.
 23. Wang, X., et al., *ARIES-ACT2 DCLL power core design and engineering*. Fusion Science Technology, 2015. **67**(1): p. 193-219.
 24. Aduloju, S.C., et al., *Steady State Thermo-Mechanics of Dual Cooled Lead Lithium Blanket*

- for Fusion Nuclear Science Facility*. 19th IEEE Symposium on Fusion Engineering, 2021.
25. Smolentsev, S., et al., *Integrated Computer Modelling for a Dual Coolant Lead Lithium Blanket in the Fusion Nuclear Science Facility*. 19th IEEE Symposium on Fusion Engineering, 2021.
 26. Aiello, G., et al., *Thermal–hydraulic analysis of the HCLL DEMO blanket*. Fusion Engineering and Design, 2007. **82**(15-24): p. 2189-2194.
 27. Barabash, V.J.R., ITER, *Appendix A, Materials design limit data*. 2013.
 28. Sannazzaro, G., et al., *Development of design criteria for ITER in-vessel components*. Fusion Engineering and Design, 2013. **88**(9-10): p. 2138-2141.
 29. Shim, H.-J., et al., *Comparative evaluation of structural integrity for ITER blanket shield block based on SDC-IC and ASME code*. Fusion Engineering and Design, 2016. **109**: p. 789-794.
 30. Huang, Y., et al., *Thermo-structural design of the European DEMO water-cooled blanket with a multiscale-multiphysics framework*. Fusion Engineering and Design, 2018. **135**: p. 31-41.
 31. Kim, D.-H., et al., *Thermo-hydraulic performance analysis for conceptual design of ITER blanket shield block*. Fusion Science and Technology, 2011. **60**(1): p. 118-122.
 32. Aduloju, S.C. and T.J. Truster, *A variational multiscale discontinuous Galerkin formulation for both implicit and explicit dynamic modeling of interfacial fracture*. Computer Methods in Applied Mechanics Engineering, 2019. **343**: p. 602-630.
 33. Aduloju, S.C. and T.J. Truster, *Primal interface debonding formulation for finite strain isotropic plasticity*. Mechanics Research Communications, 2021. **112**: p. 103606.
 34. Dai, Y., B. Long, and Z.F. Tong, *Tensile properties of ferritic/martensitic steels irradiated in STIP-I*. Journal of nuclear materials, 2008. **377**(1): p. 115-121.